

Mamba-based Deep Learning Approaches for Sleep Staging on a Wireless Multimodal Wearable System without Electroencephalography

Andrew H. Zhang^{† 1 2 3} ✉ Alex He-Mo^{† 1 2} ✉ Richard Fei Yin^{† 1 2} ✉
 Chunlin Li¹ Yuzhi Tang¹ Dharmendra Gurve² Veronique van der Horst⁵
 Aron S. Buchman⁶ Nasim Montazeri Ghahjaverestan^{2 7} Maged Goubran^{1b 2b}
 Bo Wang^{1bc 3 4} Andrew S. P. Lim^{1a 2a} ✉

¹University of Toronto Dept. of ^aMedicine, ^bMedical Biophysics, ^cComputer Science Toronto, ON, Canada

²Sunnybrook Research Institute ^aDept. of Medicine Neurology Div., ^bPhysical Sciences Toronto, ON, Canada

³Vector Institute Toronto, ON, Canada

⁴University Health Network Toronto, ON, Canada

⁵Beth Israel Deaconess Medical Center Boston, MA, USA

⁶Rush University Medical Center Chicago, IL, USA

⁷Queen's University Dept. of Electrical & Computer Engineering Kingston, ON, Canada

✉ {andrewh.zhang, alex.hemo, r.yin}@mail.utoronto.ca
 andrew.lim@utoronto.ca

Abstract

Study Objectives

We investigate Mamba-based deep learning approaches for sleep staging on signals from ANNE One (Sibel Health, Evanston, IL), a non-intrusive dual-module wireless wearable system measuring chest electrocardiography (ECG), accelerometry, and temperature, and finger photoplethysmography (PPG) and temperature.

Methods

We obtained wearable sensor recordings from 360 adults undergoing concurrent polysomnography (PSG) at a tertiary care sleep lab. Each PSG recording was manually scored and these annotations served as ground truth labels for training and evaluation of our models. PSG and wearable sensor data were automatically aligned using their ECG channels with manual confirmation by visual inspection. We trained Mamba-based models with convolutional-recurrent neural network (CRNN) and the recurrent neural network (RNN) architectures on these recordings. Ensembling of model variants with similar architectures was performed.

Results

Our best approach, after ensembling, attains a 3-class (wake, non rapid eye movement [NREM] sleep, rapid eye movement [REM] sleep) balanced accuracy of 84.02%, F1 score of 84.23%, Cohen's κ of 72.89%, and a Matthews correlation coefficient (MCC) score of 73.00%; a 4-class (wake, NREM stage 1/2 [N1/N2], NREM stage 3 [N3], REM) balanced accuracy of 75.30%, F1 score of 74.10%, Cohen's κ of 61.51%, and MCC score of 61.95%; a 5-class (wake, N1, N2, N3, REM) balanced accuracy of 65.11%, F1 score of 66.15%, Cohen's κ of 53.23%, MCC score of 54.38%.

Conclusions

Deep learning models can infer major sleep stages from the ANNE One, a wearable system without electroencephalography (EEG), and can be successfully applied to data from adults attending a tertiary care sleep clinic.

Keywords: Deep Learning Sleep Staging Wearable Devices

[†]These authors contributed equally.

1 Introduction

1.1 Sleep Staging and Polysomnography

Sleep is essential to physical and mental health. Quantitative evaluation of sleep architecture and physiology is central to the diagnosis of many sleep disorders and plays an important role in evaluating individuals with and at risk for neurodegenerative diseases [1]. Sleep is traditionally and most reliably measured by polysomnography (PSG), in which brain activity, eye movements, heart rate (HR), muscle tone, and breathing patterns are recorded simultaneously using sensors attached to a patient sleeping in a laboratory environment. This is followed by sleep staging, the manual categorization of time periods into different sleep stages based on a trained sleep technician’s visual inspection of the collected physiological data. The exact sleep staging methodology depends on the specific framework; under the American Academy of Sleep Medicine’s (AASM) [2] conventions, recordings are divided into 30-second windows, or "epochs", with electroencephalography (EEG), electromyography (EMG), and electro-oculography (EOG) used to classify epochs into three stages: awake, rapid eye movement (REM) sleep, and non-REM (NREM) sleep, which can be further subcategorized as N1, N2, and N3 sleep, with N1 as the lightest and N3 as the deepest NREM sleep. EEG is the principal signal used for sleep staging [2, 3, 4].

1.2 Wearable Devices and Automated Sleep Staging

The need for specialized personnel, equipment, and laboratory space makes PSGs expensive to conduct and difficult to scale. The cumbersome sensor setup and unfamiliar resting environment may discomfort patients, resulting in sleep that is unrepresentative of that in the home environment. Particularly sick or frail older adults may be physically unable to attend in-laboratory PSG, in addition to those living in rural or remote areas without PSG services. Furthermore, monitoring patients throughout the night and visually labelling sleep epochs is a time-consuming process that limits the throughput of sleep analyses.

In response to these challenges, wearable devices have been developed that record a subset of conventional PSG signals. Devices recording EEG have the advantage of directly measuring brain activity but the disadvantage of the discomfort associated with sensors on the head similar to PSGs. On the other hand, EEG-less devices are less obtrusive and easily set up for in-home use without a technician, but infer rather than directly measure sleep stage.

There has been considerable interest in pairing wearable devices with automated sleep stage inference in order to minimize the need for specialized technologists for labeling and hence improve scalability. Indeed, even for the analysis of conventional in-laboratory PSG, automated sleep staging has been explored as a means of addressing the time-intensiveness of sleep epoch labelling. The focus on pattern recognition and loosely rule-based nature of sleep staging is ideal for machine learning approaches which have employed model architectures like convolutional neural networks (CNNs) [5], recurrent neural networks (RNNs) [6], hybrids of the previous two (e.g. convolutional recurrent neural networks (CRNN)) [7], transformers [8], and graph neural networks [9]. Deep learning models trained on PSG data, most notably the EEG signal or some combination of EEG, EMG, and EOG, have surpassed inter-scorer agreement levels, with 5-class accuracy and Cohen’s κ as high as 92% and 86% respectively, and can make predictions orders of magnitude faster than a human evaluator at the cost of sacrificed interpretability [10, 11].

1.3 Recurrent Neural Networks and Mamba

RNNs are a class of neural networks that takes in a sequence of vectors (e.g. a time series of pulse waves, or breathing) and produce a vector output per input, allowing them to execute a wide breadth of time-series tasks. Prevalent modern RNN architectures include long short term memory (LSTM) [12] and gated recurrent units (GRU) [13], which are known to forget very long-range dependencies and whose architecture cannot take advantage of GPU acceleration, limiting the training speed.

Mamba [14] provides a solution to both problems as a type of state space model (SSM) [15] that combines the excellent long-range dependency modeling of SSMs with an additional time-dependent selection mechanism that allows for focusing on or ignoring particular features, as well as a hardware-friendly algorithm that provides computational efficiency. Empirically, Mamba has achieved state-of-the-art performance on supervised and unsupervised metrics using datasets of text, audio waveforms, and DNA sequences [14], while Mamba-based models have been adopted to perform automatic sleep staging using EEG and other PSG signals to high degrees of accuracy [16, 17].

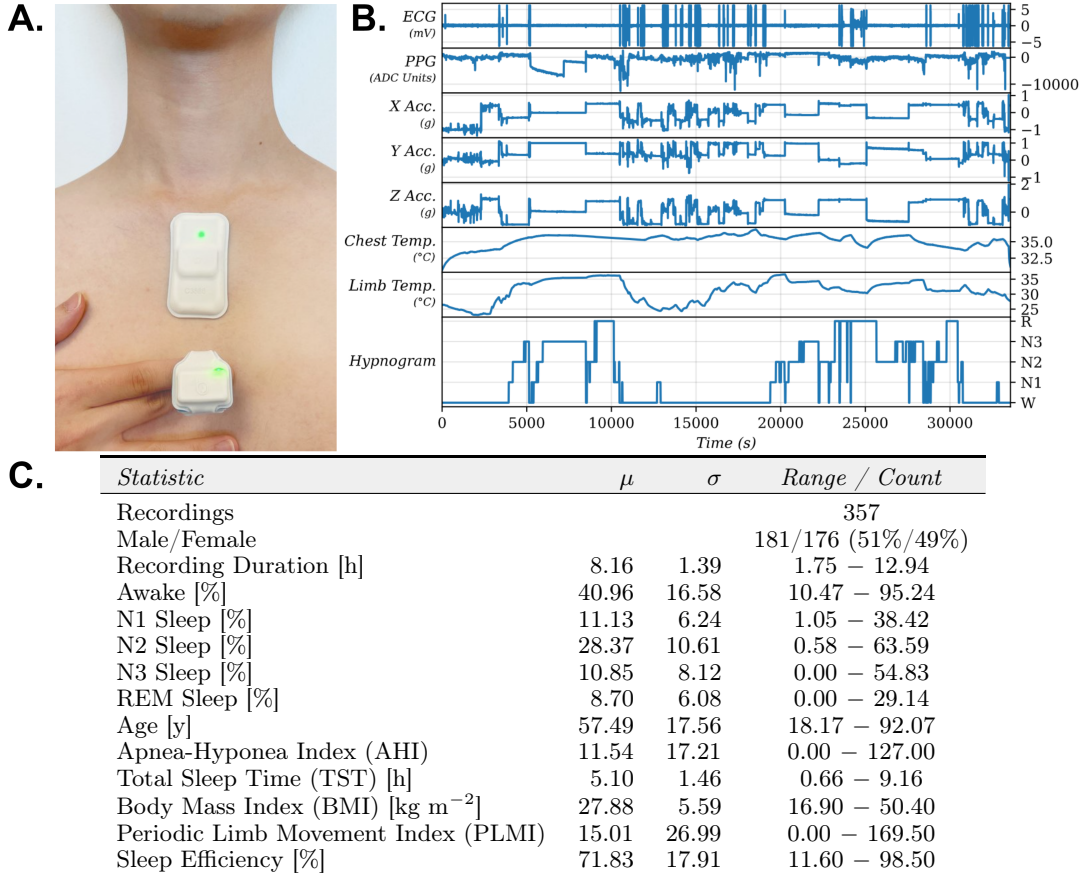


Figure 1. **A.** The finger and chest modules of ANNE One. **B.** Raw physiological signals recorded by ANNE One during a full night sleep recording and its accompanying hypnogram. **C.** Demographics and sleep characteristics of the subjects used in this study.

1.4 Contribution

This paper applies Mamba-based deep learning approaches to the problem of sleep staging using data from the ANNE One [18] sensor. ANNE One, as seen in Figure 1A, is a flexible, minimally-intrusive, and clinical-grade wireless dual-module wearable system by Sibel Health composed of a finger module, which measures photoplethysmography (PPG) and temperature, and a separate module attached to the chest via an adhesive, which measures electrocardiography (ECG), triaxial accelerometry, and temperature. The raw signals of a typical recording are plotted in Figure 1B alongside its hypnogram.

A prior study centered on ANNE One [19] exists, which primarily emphasized the development of person-specific models which were trained and evaluated on data from the same patient, with a population model trained and evaluated on data from different patients showing much poorer performance. We aim to develop a superior population model to achieve accurate sleep staging from ANNE One signals recorded from previously unseen patients.

There is a considerable body of work applying machine learning to the problem of sleep stage inference from non-EEG signals. For the most part, these have been trained and tested using the cardiopulmonary sensors of conventional PSG [20, 21, 22, 23, 24, 25, 26], which are typically artifact-free. Relatively few studies have applied these approaches to data from wearable devices, which are in general more prone to poor signal quality and signal loss; consequently, such studies often need to reject epochs of poorer-quality signal prior to model training and prediction. Moreover, these works have focused on analysis of data from single sensors, typically ECG or PPG [27, 28]. Finally, models developed for wearable sensors have largely trained on data from relatively young and healthy volunteers, rather than patients presenting to sleep clinics, raising a question of generalizability to clinical populations.

The current study builds on and extends this body of work in several ways. First, we leverage the ANNE One devices’ multi-sensor nature, which may in principle allow for predictions even in settings where

one or more sensors are reading low-quality signals. Second, we train and test on data from relatively older patients with a range of sleep disorders (41% were over the age of 65 and 46% had sleep apnea; Figure 1C) rather than younger and healthier patients, ensuring applicability to older adults with sleep complaints. This is particularly important as age, sleep, and neurological conditions can all plausibly alter the relationship between sleep stage and autonomic, cardiac, and pulmonary function, meaning that models trained on younger adults may generalize poorly to older adults. Finally, this work broadens the Mamba architecture to EEG-less sleep staging by exploring whether Mamba’s relative performance increases [16, 17] are also noticed in this context.

2 Method

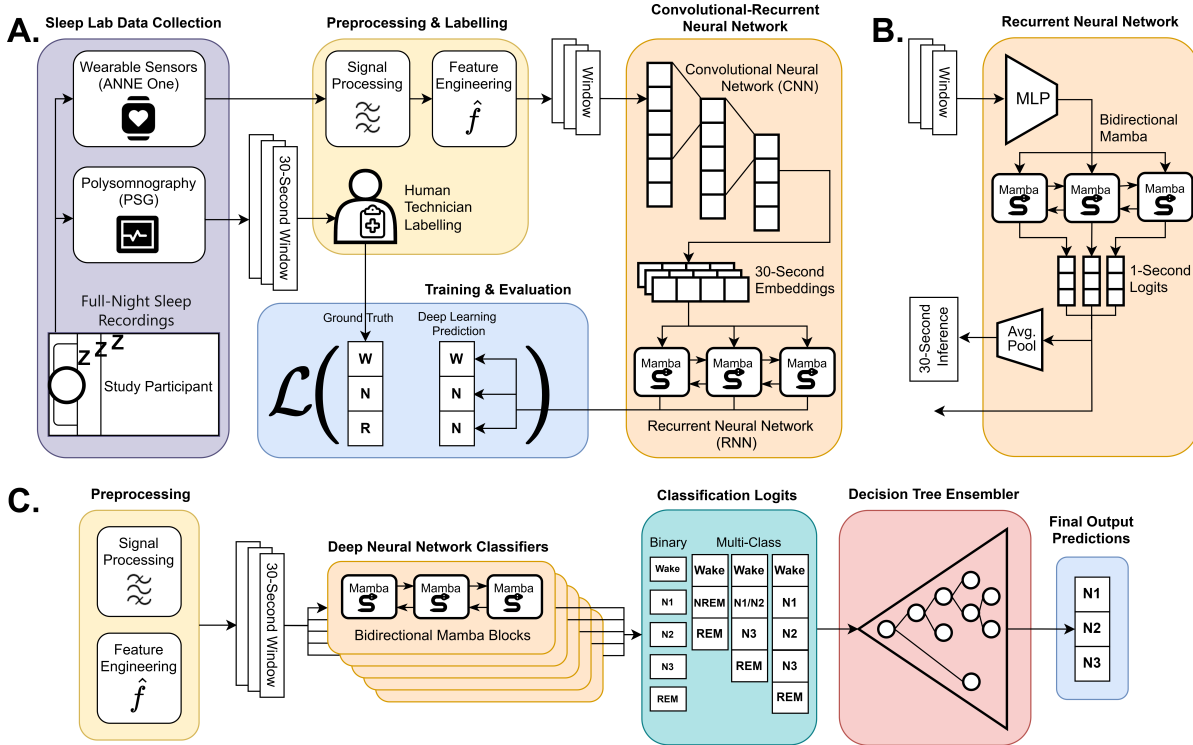


Figure 2. Overview of deep learning pipelines of this study. **A.** The training pipeline with the CRNN architecture. **B.** The RNN architecture. **C.** The inference-time ensembling pipeline.

2.1 Dataset

ANNE wearable sensors were used to collect full-night recordings from 360 adults undergoing concurrent clinical PSG at a tertiary care clinical sleep laboratory in Sunnybrook Health Sciences Centre, Toronto, Canada. PSGs were recorded according to AASM practice parameters for in-laboratory PSGs with a Grael PSG system (Compumedics, Victoria, Australia). The study was conducted in accordance with the latest version of the Declaration of Helsinki. All subjects provided written informed consent for the full study protocol.

Participants were first instrumented with the ANNE One, whose recordings were started ahead of the set-up and initiation of PSG recordings. In order to mimic what would occur in a home environment, the ANNE signals were not monitored in real time, and no attempt was made to correct sensor-related issues (e.g. poor skin contact) overnight. Upon completion, each PSG recording was manually labeled by one of four technologists according to AASM standards [2]. In addition, the portion of the ANNE recordings preceding the onset of PSG recording was labeled as wake based on direct observation of participants by study staff. PSG and wearable sensor data were automatically aligned by their shared ECG signals using cross-correlation analysis and verified by visual inspection.

Three participants who did not sleep at all were excluded from analysis, as were time periods prior to the sensor placement or after the sensors were taken off, leaving a total of 357 patients with 2914 hours of recording. The characteristics of the study’s participants are outlined in Figure 1C. Generally, older participants (age ≥ 65) and those with sleep apnea had poorer sleep quality, with lower total sleep time, poorer sleep efficiency, and increased N1 sleep time relative to other sleep stages (Appendix A).

The machine learning task is defined from the dataset as a form of multiclass 1D signal segmentation, wherein the ANNE One signals constitute the features, the PSG-annotated sleep stages form the labels, and class predictions are made per point in time, as demonstrated in Figure 2A.

2.2 Preprocessing

The ECG data were recorded at 512 Hz and preprocessed as follows. A wavelet transform was applied to raw ANNE ECG signals to identify temporal windows containing QRS complexes; within each window, raw ECG signals were searched for local maxima and minima to identify the precise timing of the R-peak. The wavelet-transformed ECG data were subsequently downsampled to 100 Hz for additional analyses. For each peak, morphological features (e.g. amplitude, sharpness) were extracted and hierarchical density-based spatial clustering of applications with noise (HDBSCAN) [29] served to group all identified peaks into a small number of clusters. Peaks occurring in trains with relatively stable RR intervals in the physiological range of human HR were identified as likely representing physiological QRS complexes. QRS complexes that clustered morphologically with these peaks, irrespective of regularity, were used to compute beat-to-beat heart rate.

The PPG data were recorded at 128 Hz and preprocessed as follows. First, PPG signals were band-pass filtered between 0.5 – 5 Hz and downsampled to 100 Hz. Trains of physiological pulse waves were identified on the basis of relatively stable HR and amplitude. These high-quality pulse waves were normalized to a standard amplitude and duration, and clustered using HDBSCAN. For each cluster, the mean of its normalized pulse waves was taken as a template wave for that cluster; beat-to-beat template matching was performed to determine the extent to which each pulse wave in the rest of the recording matched one of the template waves, with the lowest sum-squared similarity to the template constituting a measure of signal quality for each PPG pulse wave. For each matching pulse wave, the timing of the foot and peak was noted, from which a measure of heart rate was obtained.

The pulse arrival time (PAT) is the delay from the R-peak of the ECG to the arrival of the pulse wave in the PPG. To compute PAT from the ANNE data, the time-series of valid ECG peaks and PPG feet were matched to each other by empirically considering all possible lags within the range 0 – 1000 msec and selecting that which successfully matched the greatest number of ECG peaks and PPG feet. Afterwards, for each ECG R-peak and its corresponding PPG foot, the PAT of that heartbeat was computed, generating a beat-to-beat time series of PAT.

The chest XYZ accelerometry data were recorded at 210 Hz and low-pass filtered, followed by the computation of the euclidean norm minus one (ENMO), theta (body pitch), phi (body roll) and the z-angle (the deviation from vertical of a vector perpendicular to the face of the sensor).

2.3 Model

Two Mamba-based deep neural network architectures were investigated: a convolutional-recurrent neural network (CRNN) and a recurrent neural network (RNN) as summarized in Figures 2AB, 3. The CRNN is a typical sleep stage architecture [21, 11] that emulates the way human evaluators label PSGs: the convolutional component encodes physiological signals within each epoch while the recurrent component captures transitional relationships between sleep stages across epochs. The RNN architecture is a lightweight and parameter-scarce alternative to the CRNN, consisting of $\times 8$ less parameters ($\approx 580K$ vs. $\approx 70K$). Since Mamba is designed for long-context pattern recognition, it could potentially interact with signals more effectively than the CRNN if given them directly without windowing.

The CRNN architecture has three input channels for *time-series*, *frequency*, and *scalar* data (see Figure 3): the first two are 3D inputs, with axes for the number of 30-second windows (mirroring the 30-second windows used in visual annotation of PSG data according to AASM criteria), the window size (i.e. 30 seconds worth of sequential data), and number of features, while the 2D scalar inputs have axes for the number of windows and number of features. The model comprises:

- 1) A convolutional component, consisting of 1D residual blocks that sequentially downsize the time-series and frequency datas' window size axes and flatten them into an embedding vector per window. The time-series embedding, frequency embedding and scalar data are then concatenated across the feature axis to form an embedding vector per window.
- 2) A recurrent component, consisting of a bidirectional three-layer Mamba block that processes the embedding vectors sequentially, followed by an element-wise multi-layer perceptron (MLP) that diminishes the feature-size axis into logits for each class. The bidirectional Mamba block (Appendix B) is the concatenation of two Mamba blocks that process epochs in opposite directions, allowing for a widened receptive field to detect patterns in signals more effectively.

The RNN architecture (Figure 2B) processes a single 2D input channel with axes for the number of n -second windows and number of features, where $n = 1$ is an arbitrary value dividing 30. It comprises:

- 1) An element-wise MLP with $h = 100$ hidden layer dimensions that downsizes the data to $k = 10$ dimensions, where the choices of h and k are arbitrary.
- 2) A bidirectional three-layer Mamba block that processes windows sequentially.
- 3) An element-wise MLP that downsizes the data into logits, which, during inference-time, can be grouped and averaged to form logits per 30-second window to comply with AASM standards.

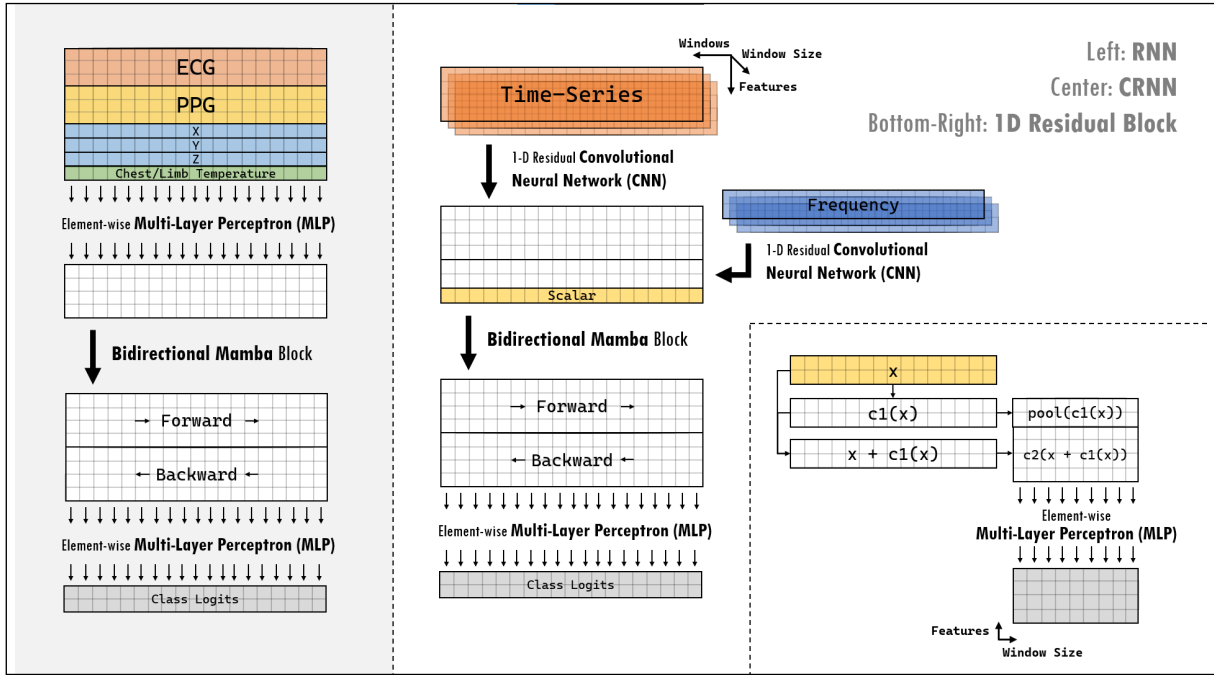


Figure 3. Implementation of deep neural network architectures and substructures used in this study. $c1$ and $c2$ are 1D convolutions with same-size padding. $c2$ has a stride of 2 and $2\times$ more output features than input features.

Our previous investigations [30] (Appendix C) have found engineered frequency domain and scalar features to yield significant performance benefits for GRU-based deep learning approaches. The engineered scalar features, which have also shown discriminatory value in other previous models [30], distribute differently depending on sleep stage, while changes to their frequency domains often designate sleep stage transitions (Appendix D). Thus, empirical selections of these features (Table 1) were introduced along with the time-series signals for both the CRNN and RNN.

A series of transformations were applied to further adjust the preprocessed data to the individual architectures. For the CRNN, all signals were resampled to 25 Hz and grouped to N 30-second windows, resulting in $25 \times 30 = 750$ data points per window. Then, depending on feature type (see Table 1),

- For *time-series features*, the signal was left alone.

- For *frequency features*, the log-magnitude spectrum was taken of the detrended signal over the 30-second axis.
- For *scalar features*, the signal was reduced over the 30-second axis. Metadata, in the form of patient age and sex (male = 0, female = 1), was incorporated into the scalar features by repeating the constants N times throughout the recording.

For the RNN, the accelerometry, ECG, and PPG signals were detrended, with the accelerometry signals further band-pass filtered over 0.005 – 0.2 Hz. Log-magnitude spectrograms were taken with a window size of 100 points and no overlap, then finally concatenated with limb/chest temperature, which was resampled to 1 Hz, and sleep stage label, of which each point was repeated 30 times to 1 Hz.

Table 1. Features used by the RNN and CRNN models and their categorization. An asterisk (*) after a feature means the feature’s frequency spectrum is used.

<i>RNN</i>	<i>CRNN</i>		
	Time-Series	Frequency Scalar	
ECG*	Heart Rate (ECG + PPG)	ECG*	Age
PPG*	Heart Rate (ECG)	PPG*	Sex
X*	Heart Rate (PPG)	X*	Mean, ECG SQI
Y*	Pulse Arrival Time (PAT)	Y*	Mean, PPG SQI
Z*	Euclidean Norm Minus One (ENMO) ¹	Z*	Entropy, PPG
Chest Temperature	Z-Angle ²	Z-Angle*	Entropy, PPG*
Limb Temperature	Limb-Chest Temperature Difference		Skew, PPG*
	Theta		Scale, Heart Rate (ECG + PPG)
	Phi		Kurtosis, ENMO
			Entropy, Z-Angle

2.4 Training

The training, validation, and testing sets were randomly split in a 75%/10%/15% ratio to sizes 267/36/54. During the training process, recordings were clipped to random segments to prevent the model from overfitting to the high-level structure of most recordings, i.e., wake periods at the start and end with sleep in the middle. Cross-entropy loss was used, weighted on inverse class frequency to adjust for the moderate class imbalance as encapsulated by Figure 1C. The model from the training epoch that maximized balanced validation accuracy was chosen as the final model. Both CRNN and RNN models were trained with Adam [32], a widely-used adaptive learning rate optimizer.

The CRNN model was trained on single batches. Recordings were clipped to segments of size varying uniformly between $\lceil \frac{N}{10} \rceil$ and N , and age/sex values individually were set to -1 with probability 0.3, an arbitrary value, as a form of data augmentation. The RNN model was trained on a batch size of 4, with recordings clipped randomly to sequence lengths of 5000 seconds.

Three models of varying sleep stage resolution were built: a 3-class, 4-class, and 5-class sleep staging model. The 5-class model has classes for wake, N1, N2, N3, and REM sleep, while the 3-class model groups N1, N2, and N3 sleep into non-REM sleep. The 4-class model designates N1 and N2 sleep as "light sleep" as opposed to N3 or "deep sleep", a common practice in automatic sleep staging [4].

2.5 Ensembling

For each of the n classes inside a n -class ensemble model, a binary model was trained to predict the presence or absence of that class. The logits of these binary models were stacked with logits from the regular n -class models to form the inputs to a suite of decision tree-based architectures including AdaBoost [33], random forests [34], extra-tree classifiers [35], histogram gradient boosting [36], and XGBoost [37]. The model among the suite that maximized balanced validation accuracy was selected as the final ensembler model. A visual representation of the ensembling pipeline is presented in Figure 2C.

¹Euclidean Norm Minus One (ENMO) is calculated as $\sqrt{x^2 + y^2 + z^2} - 1$

²Z-angle is calculated as $\arctan\left(\frac{z}{\sqrt{x^2 + y^2}}\right)$ [31]

2.6 Statistical Analyses

Results were compiled of 3-class, 4-class, and 5-class sleep staging for the RNN and CRNN architectures and for regular and ensemble models. Overall performance was evaluated by aggregating all test set recordings and computing the balanced accuracy, weighted precision, weighted recall, weighted F1, Cohen’s Kappa (κ), and Matthews correlation coefficient (MCC).

For the best model type, performance was plotted on a healthy subset of the test set and ablation studies are carried out using various subsets of the ANNE One sensor data and a different sequential architecture. For the best 5-class model, Blant-Altman plots were created to evaluate class-wise biases, followed by analyses of averaged per-recording metrics both individually and across clinical variables including age, sex, PLMI, AHI, BMI, TST, and sleep efficiency. Because individual recordings do not necessarily contain instances of all five sleep stages, balanced accuracy may not be a sensible metric for recording-wise comparisons; hence, accuracy was presented in lieu of balanced accuracy for those cases.

3 Results

3.1 Model Evaluation

Typical-case recording predictions for all 5-class models are shown in Figure 4 along with predicted point-wise output class probabilities for models that can produce them. A Uniform Manifold Approximation and Projection (UMAP) [38] of an intermediate CRNN output is also provided in Appendix E, which shows the separation of sleep stages as clusters in the learned representation space.

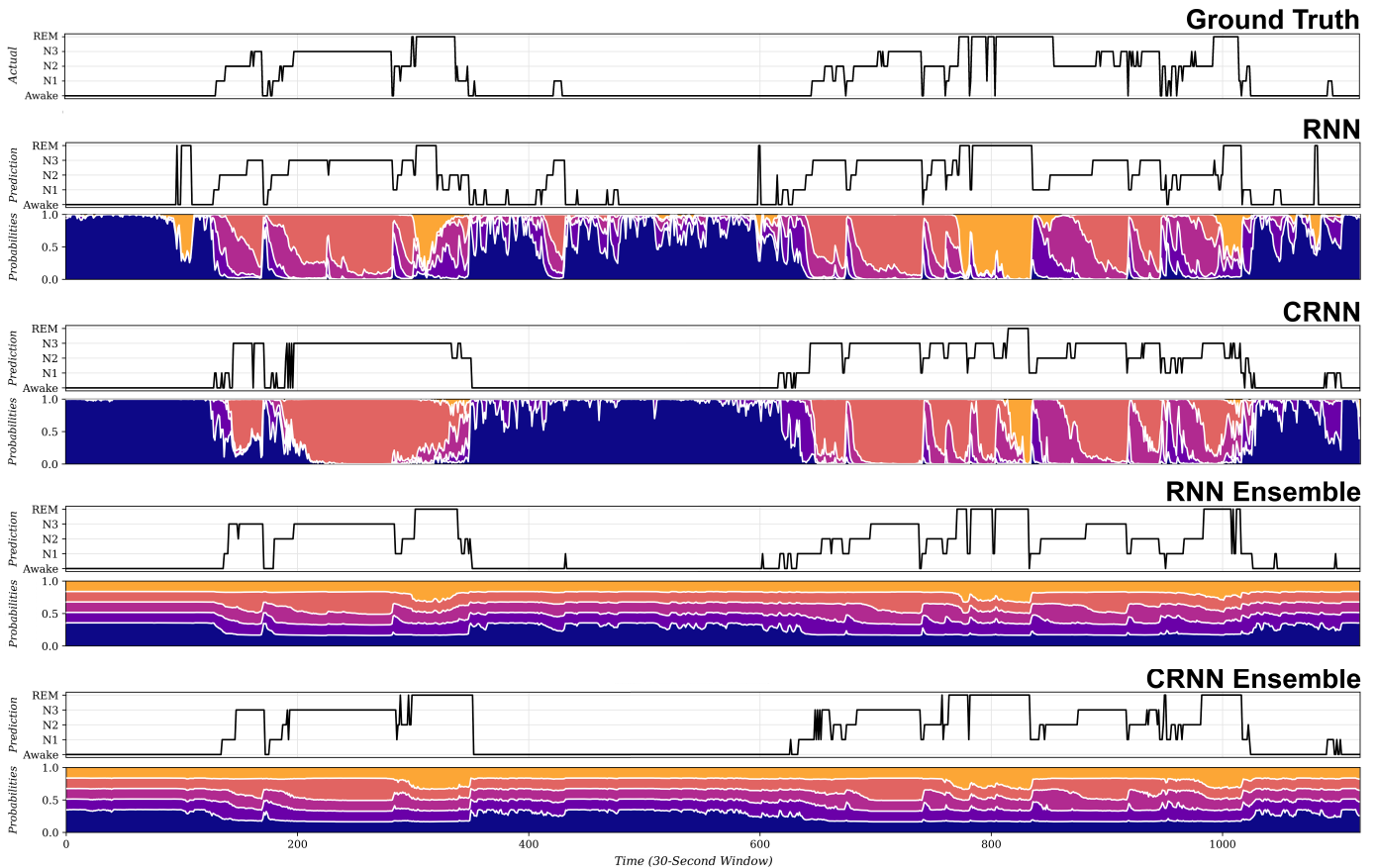
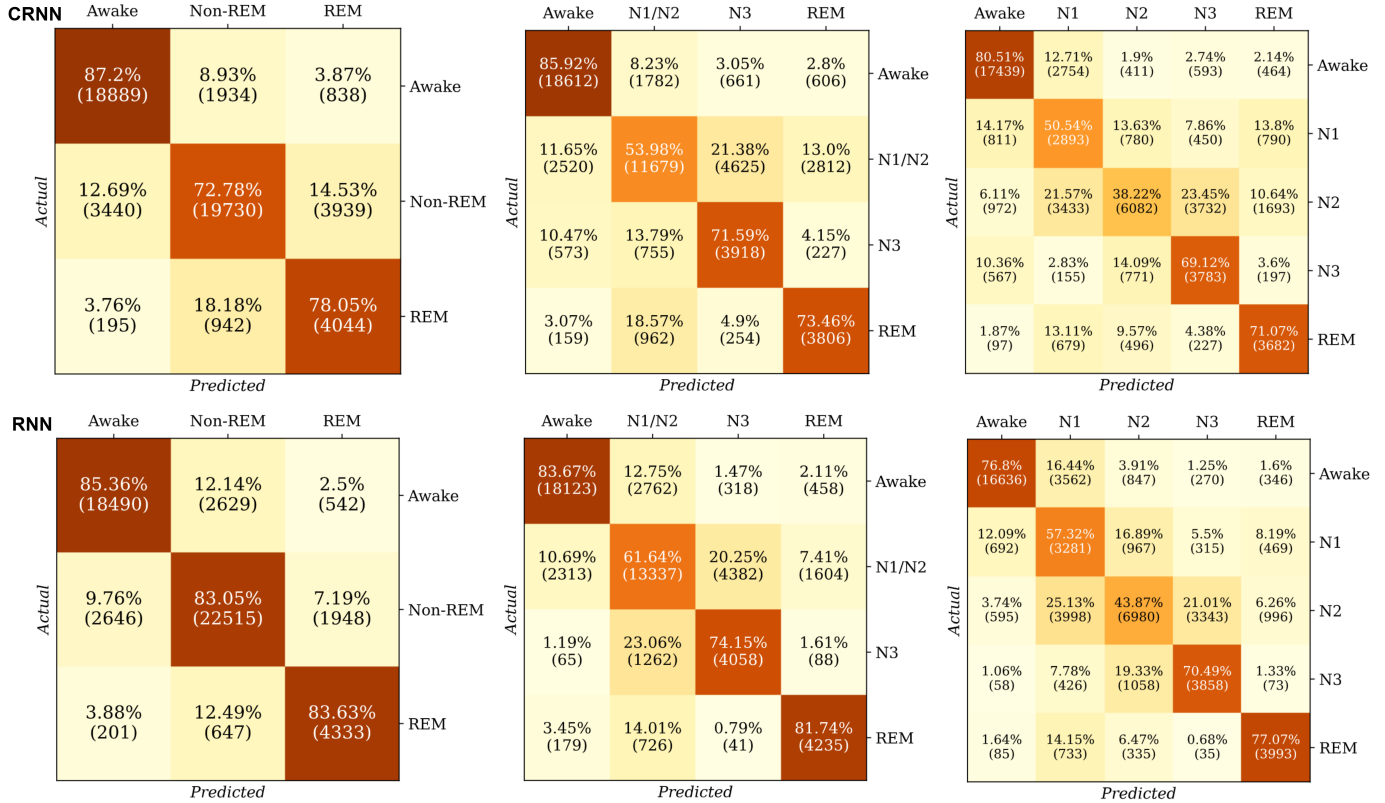


Figure 4. 5-class regular and ensemble model predictions and class probabilities for a single full-night recording in the test set. The regular models show softmax probabilities, while the ensemble models show decision tree probabilities. A UMAP of the CRNN model learned embeddings for the same recording is also provided in Appendix E. Probabilities are coloured by ground truth sleep stage: darker to lighter colours represent wake to REM sleep.

Figure 5 displays the confusion matrices for all n -class ensemble models and overall metrics across all n -class regular and ensemble models. No meaningful deviations in performance were observed in the RNN models as tested on 1-second windows and as tested on 30-second windows (balanced accuracies of 1-second RNN ensembles are 83.74%, 75.06%, 64.86% for 3/4/5-class models), of which the latter is presented in this paper. The RNN ensemble model yields the best metrics and dominates most class-wise metrics (5-class balanced accuracies of 86.19%, 69.62%, 67.72%, 81.16%, and 86.60% for wake, N1, N2, N3, and REM sleep respectively, Appendix F). Ensemble models perform better than their single-model counterparts, while RNNs perform better than the CRNNs despite the shallower feature set and smaller parameter count. Most misclassifications are made between N1 and every other class, as well as between N2 and N3 for 5-class sleep staging.



Classes	Model	Metric (%)					
		Balanced Accuracy	Precision	Recall	F1	Cohen's κ	MCC
5	CRNN	55.47	63.24	59.25	59.84	45.50	46.16
	RNN	60.20	69.48	61.20	63.68	49.16	50.18
	CRNN Ensemble	61.89	68.86	62.80	63.58	50.86	51.93
	RNN Ensemble	65.11	71.61	64.41	66.15	53.23	54.38
4	CRNN	65.84	69.47	67.72	67.18	52.34	53.32
	RNN	67.59	73.08	66.59	68.34	51.95	53.06
	CRNN Ensemble	71.24	74.14	70.46	70.89	57.40	58.35
	RNN Ensemble	75.30	75.80	73.68	74.10	61.51	61.95
3	CRNN	64.25	71.95	69.79	69.02	48.45	50.43
	RNN	81.09	83.20	81.98	82.35	69.59	69.77
	CRNN Ensemble	79.35	81.93	79.08	79.76	65.48	66.17
	RNN Ensemble	84.02	84.76	84.04	84.23	72.89	73.00

Figure 5. Test set confusion matrices of ensembled CRNN and RNN architecture models for 3, 4, and 5 class sleep staging (top); Macro-evaluation metrics for all n -class models on the test set (bottom), where the best-performing model for each metric is bolded.

In a set of young and healthy sleepers (age < 40, AHI < 5, PLMI < 5), the RNN ensemble model experiences a significant boost in performance as denoted in Figure 6 although removal of these participants from the test set does not substantially worsen model performance, indicating that overall model performance is not driven by these healthy participants (Appendix G, Figure 12).

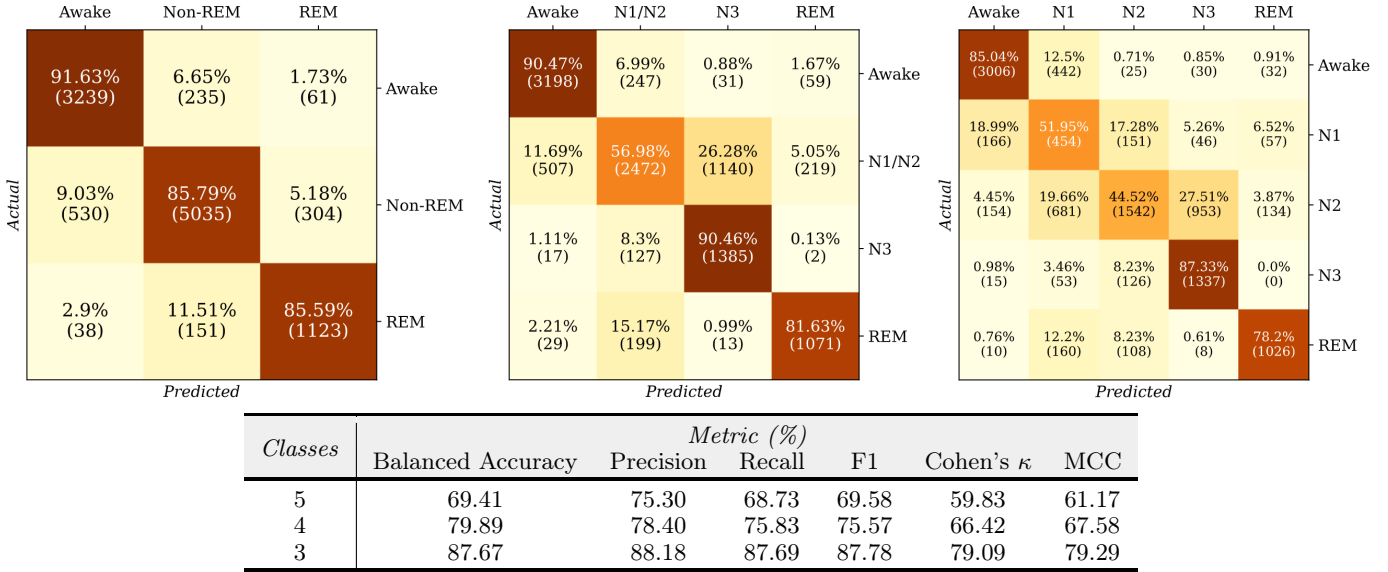


Figure 6. Confusion matrices and macro-evaluation metrics of 3-class, 4-class, and 5-class RNN ensemble models on a healthy subset of the test set ($n = 11$) defined as age < 40 and AHI < 5 and PLMI < 5.

3.2 Feature Ablation Study

We next investigated which sets of sensors (chest module vs. limb module; ECG vs. PPG vs. other) were most influential to model performance. To do so, modified instances of the RNN ensemble model were trained to determine the utility of its components. Firstly, feature sets solely from the ANNE One’s chest module (ECG, accelerometry, chest temperature) or limb module (PPG, limb temperature) were examined. As shown in Table 2, the chest-only model trails closely behind the original in performance while the limb-only model exhibits a marked degradation ($\approx 10\%$) for all metrics. This strongly suggests that the chest module is the principal driver behind model accuracy, although the limb module alone is capable of recovering sleep staging information to a rough degree. Next, because the ECG and PPG sensors themselves are the most likely to experience poor signal quality, we examined the performance of RNN ensemble models trained on only the accelerometry and temperature sensors. Remarkably, exclusion of ECG and PPG data resulted in minimal loss of accuracy, meaning that information in the ECG and PPG is also being captured effectively by the accelerometry signals.

Table 2. Evaluation metrics for the 3-class, 4-class, and 5-class RNN ensemble models using different subsets of the entire feature set. The best-performing model for each metric is bolded.

Classes	Feature Set	Metric (%)					
		Balanced Accuracy	Precision	Recall	F1	Cohen's κ	MCC
5	Full	65.11	71.61	64.41	66.15	53.23	54.38
	Chest Module	63.94	70.66	62.63	64.22	51.23	52.59
	Limb Module	54.83	62.29	55.08	56.56	41.60	42.59
	No ECG/PPG	63.85	70.68	63.35	65.03	51.97	53.12
4	Full	75.30	75.80	73.68	74.10	61.51	61.95
	Chest Module	73.46	74.63	71.64	72.26	58.88	59.47
	Limb Module	64.89	68.63	63.59	64.66	48.22	49.13
	No ECG/PPG	73.03	74.46	71.52	72.10	58.70	59.30
3	Full	84.02	84.76	84.04	84.23	72.89	73.00
	Chest Module	81.77	83.58	82.50	82.83	70.39	70.53
	Limb Module	73.28	78.10	74.71	75.84	58.21	58.69
	No ECG/PPG	82.78	84.26	83.18	83.51	71.71	71.56

3.3 Recurrent Architectures

In order to understand whether the incorporation of Mamba improved the RNN ensemble model, a similarly-sized variant model replacing Mamba with LSTM was trained, its results provided by Table 3. The LSTM model shows a minor loss in all metrics, confirming the Mamba approach is beneficial.

Table 3. Evaluation metrics for the 3-class, 4-class, and 5-class RNN ensemble models using Mamba and LSTM blocks. The best-performing model for each metric is bolded.

Classes	Architecture	Metric (%)					
		Balanced Accuracy	Precision	Recall	F1	Cohen’s κ	MCC
5	Mamba	65.11	71.61	64.41	66.15	53.23	54.38
	LSTM	62.64	69.46	62.47	64.03	50.76	51.87
4	Mamba	75.30	75.80	73.68	74.10	61.51	61.95
	LSTM	72.82	73.95	71.64	72.06	58.70	59.17
3	Mamba	84.02	84.76	84.04	84.23	72.89	73.00
	LSTM	81.06	82.90	81.37	81.82	68.71	68.95

3.4 Global Sleep Metrics

As a means of evaluating model bias and verifying model robustness, Figure 7 lays out scatter plots and Bland-Altman plots for the 5-class RNN ensemble, comparing RNN predicted vs. PSG actual values for a number of summary metrics including time asleep, % N1 sleep, % N2 sleep, % N3 sleep, and % REM sleep. The model trends towards slightly underestimating wake and N2 sleep and slightly overestimating N1 and N3 sleep.

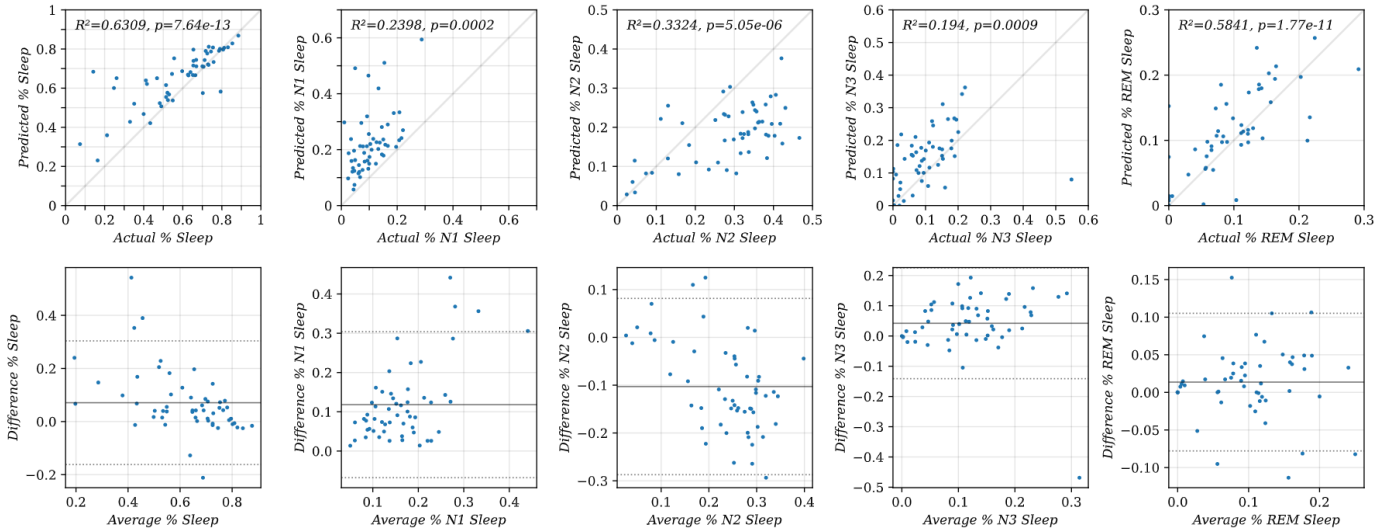


Figure 7. Predicted vs. actual sleep stage scatter plots (top row) and Bland-Altman plots (bottom row) for the 5-class RNN ensemble model on the test set. The center horizontal line is the mean. The two dotted lines are 1.96 standard deviations above and below the mean.

3.5 Performance by Clinical Group

Averaged recording-wise metrics are catalogued in Table 4 for the 5-class RNN ensemble, wherein linear regressions were performed to fit various recording metrics to accuracy (plots in Appendix G, Figure 13). Performance of the RNN ensemble is robust to differences in all metrics except AHI, which had a weak negative correlation with accuracy, though the proportion of variance in accuracy explained by AHI is modest (RNN $R^2 = 0.0751$). Four annotators were involved in generating the ground truth labels used in this study and the agreement between the RNN model and the ground truth labels did not differ by the individual who generated the annotations (RNN $p = 0.89$, one-way F-test).

Table 4. Per-recording accuracy for the 5-class RNN ensemble model (top); R^2 and slope p -values of a line fitting various sleep statistics to accuracy using linear regression (bottom). Statistically significant p -values (< 0.05) are bolded.

<i>Metric (%)</i>	μ	σ
Accuracy	64.54	10.77
F1	66.72	10.28
Cohen’s κ	50.58	14.50
Matthews Correlation Coefficient	52.92	13.40
<i>Sleep Statistic</i>	R^2	p
Age	0.0618	0.0700
Sex	0.0334	0.1861
Periodic Limb Movement Index (PLMI)	0.0338	0.1830
Apnea-Hypopnea Index (AHI)	0.0751	0.0449
Body Mass Index (BMI)	0.0350	0.1753
Total Sleep Time (TST)	0.0055	0.5940
Sleep Efficiency	0.0002	0.9281

4 Discussion

4.1 Key Findings

This work has developed Mamba-based CRNN and RNN models to accurately perform inference from the ANNE One device for major sleep stages. The models demonstrate good performance across a wide range of patient characteristics, without a need to screen and exclude recordings and epochs on the basis of signal quality, and with the RNN architecture slightly outperforming the CRNN architecture.

4.2 Related Studies

Previous studies have undertaken the challenge of inferring sleep stage from non-EEG signals (Tables 5 & 7) using a mixture of cardiopulmonary (ECG, PPG, respiratory impedance bands, respiratory flow cannulas) and accelerometry data. Many studies used data from conventional PSG recordings [20, 21, 22, 23, 24, 25, 26] although a handful of studies used data from purpose-designed wearable sensors [28, 21, 19, 23, 24, 27]. In general, models trained on and applied to PSG data performed better than models utilizing wearable sensor data. This is not surprising since signal quality is often much higher for attended in-laboratory PSGs where more intrusive sensors can be used, and signal quality is continuously monitored and issues can be addressed by the technologist as they occur. Even so, despite using wearable rather than PSG sensor data, the performance of our ensemble RNN model approached [21, 24, 25, 26, 20, 22] or exceeded [23] that of models trained on much larger sets of PSG data.

Our model exceeded the overall performance of most wearable sensor based models [27, 23, 28] with the exception of one [24]. Of note, this study examined a younger set of participants (mean age 45) who were free of psychiatric and neurological co-morbidity, which may influence the relationship between sleep stage and its autonomic, cardiac, and pulmonary manifestations. In contrast, we studied an older (mean age 57.49) set of participants with significant sleep co-morbidity (45.81% with AHI > 5). When we limit our analyses to younger individuals without sleep apnea or significant periodic limb movements, model performance improves further (Figure 6). Another contrast between [24] and the present study is that [24] performed much stricter quality control for recording quality with 54/136 or nearly 40% of nights of wearable sensor recording excluded from analysis due to poor signal quality. In contrast, in the

interest of evaluating real-world performance, we did not exclude any recording or any epochs on the basis of signal quality and the reported results reflect consideration of all available epochs of recording, irrespective of signal quality. The robustness of our model to missing data or poor signal quality is likely related in part to its use of multiple data streams, in particular accelerometry, which appeared to capture much of the information that would otherwise have been captured by ECG or PPG.

Of particular comparative interest is the one previous paper addressing sleep stage inference from ANNE One data [19]. Ultimately, success in developing a population model was limited, and while there was some success in generating person-specific models, the performance of our ensemble RNN model exceeded even the best person-specific model in the paper which had a 4-class balanced accuracy of 73.4%.

Table 5. PSG-based evaluations of sleep staging models in related literature. For papers that provided confusion matrices, additional metrics were manually calculated and included in tandem with those explicitly reported by the paper. Acc. = accuracy, B.Acc. = balanced accuracy, κ = Cohen’s Kappa.

<i>Study (Year)</i>	<i>Dataset</i>	<i>Metric</i>	<i>%</i>	<i>Signal Features</i>
Radha et al. (2019) [20]	SIESTA (7 sleep laboratories) – 584 recordings (292 subjects) – 25% testing	4-stage Acc.	77	ECG
		4-stage κ	61	
Sun et al. (2020) [21]	MGH (sleep laboratory) – 8682 recordings (7208 subjects) – 20% testing	3-stage B.Acc.	86.8	ECG + Respiratory Effort
		3-stage F1	84.2	
		3-stage κ	76.0	
		5-stage B.Acc.	70.3	
		5-stage F1	68.1	
Kotzen et al. (2022) [22]	SHHS Visit 1 (multi-center) – 5758 recordings (pretraining) MESA (general population) – 2056 recordings – 204 testing	4-stage Acc.	84	PPG
		4-stage B.Acc.	76	
		4-stage F1	83	
		4-stage κ	75	
Kotzen et al. (2022) [22]	SHHS Visit 1 (multi-center) – 5758 recordings (pretraining) CFS Visit-5 v1 (family study) – 324 recordings – 80 testing	4-stage Acc.	82	PPG
		4-stage B.Acc.	80	
		4-stage F1	82	
		4-stage κ	74	
Pini et al. (2022) [23]	Unspecified (academic sleep centers) – 12404 recordings CinC (sleep laboratory) – 994 recordings – External testing set	3-stage B.Acc.	74.0	ECG
		3-stage F1	81.4	
		3-stage κ	61.6	
		3-stage MCC	61.7	
		4-stage B.Acc.	63.6	
		4-stage F1	72.0	
		4-stage κ	53.6	
4-stage MCC	54.0			
Topalidis et al. (2023) [24]	Custom (general population w/ sleep complaints) – 314 recordings (185 subjects) – 25% testing – Ambulatory home recordings	4-stage B.Acc.	85.4	ECG
		4-stage F1	86.3	
		4-stage κ	79.2	
		4-stage MCC	79.2	
Jones et al. (2024) [25]	CCSHS, CFS, CHAT, MESA, WSC – 4000 random sampled recordings – 500 testing	5-stage B.Acc.	74	ECG
		5-stage Median κ	72.5	
Kazemi et al. (2024) [26]	UC Irvine Sleep Center – 123 recordings – 20% testing	3-stage κ	71.4	PPG + Resp. Flow Rate + Resp. Effort
		4-stage κ	55.0	
		5-stage κ	61.6	

Table 6. Wearable-based evaluations of sleep staging models in related literature. For papers that provided confusion matrices, additional metrics were manually calculated and included in tandem with those explicitly reported by the paper. Resp. = respiratory, Accel. = accelerometry, Temp. = temperature, Acc. = accuracy, B.Acc. = balanced accuracy, Prec. = precision, Rec. = recall, κ = Cohen’s Kappa, MCC = Matthews correlation coefficient.

<i>Study (Year)</i>	<i>Dataset</i>	<i>Metric</i>	<i>%</i>	<i>Signal Features</i>
Zhang et al. (2018) [28]	Beijing General Hospital of the Air Force (general population) – 39 recordings – 12.5% testing	5-stage Prec.	58.5	Heart Rate + Actigraphy
		5-stage Rec.	61.1	
		5-stage F1	58.5	
Sun et al. (2020) [21] <i>Model from Table 5</i>	SHHS Visit 1 & 2 (multi-center) – 1000 random sampled recordings – External testing set	3-stage B.Acc.	80.8	ECG + Resp. Effort
		3-stage F1	80.2	
		3-stage κ	69.7	
		5-stage B.Acc.	63.9	
		5-stage F1	58.6	
Chen et al. (2022) [19] <i>Individual-Based Model</i>	Shirley Ryan AbilityLab (inpatient unit) – 10 recordings – 10% testing	3-class Mean κ	60.0	ECG + PPG + Accel. + Temp.
		4-class B.Acc.	73.0	
		4-class Mean κ	61.7	
Chen et al. (2022) [19] <i>Population Model</i>	Shirley Ryan AbilityLab (inpatient unit) – 10 recordings – 10% testing	3-class Mean κ	17.1	ECG + PPG + Accel. + Temp.
		4-class Mean κ	6.1	
Pini et al. (2022) [23] <i>Model from Table 5</i>	Z3Pulse (general population) – 156 recordings (52 subjects) – ECG-based wearable – External testing set	3-stage B.Acc.	72.5	ECG
		3-stage F1	79.8	
		3-stage κ	61.2	
		3-stage MCC	61.4	
		4-stage B.Acc.	64.2	
		4-stage F1	69.8	
		4-stage κ	53.2	
Topalidis et al. (2023) [24] <i>Model from Table 5</i>	Custom (general population w/ sleep complaints) – 314 recordings (185 subjects) – 25% testing	4-stage B.Acc	84.4	ECG, PPG
		4-stage F1	83.9	
		4-stage κ	76.2	
		4-stage MCC	76.3	
Silva et al. (2024) [27]	Instituto do Sono (general population) – 1522 recordings (1430 subjects) – 586 testing	4-stage Mean Acc.	70.7	Heart Rate + Accel.
		4-stage Mean κ	56	

4.3 Model Performance

Both CRNN and RNN model architectures obtain maximal per-class performances for wake and REM, and minimal per-class performances for N1 and N2 sleep. As a transitory state, periods of N1 sleep are short and instable, making its discrimination a difficult task. Physiological similarities between N2 and N3 sleep, such as cardiorespiratory signatures, similarly complicate the model’s ability to differentiate them, as evidenced by N2-N3 confusion as the most frequent misprediction for 5-class models (as well as N1/N2-N3 confusion for 4-class models). Ultimately, the differences between N1, N2, and N3 represent a matter of depth rather than kind, and some degree of difficulty in distinguishing these without EEG is to be expected. Conversely, wake and REM sleep have clearer differentiating characteristics, such as higher heart rate, which allows for easier classification.

In spite of a simpler feature set and smaller parameter count, the RNNs outperform the CRNNs in virtually every metric. It is possible that the independent processing of segmented windows by the CNN component interfered with the wider CRNN’s ability to discern changes at neighbouring window boundaries. As well, during epochs where sleep is transitioning between classes, the provided label becomes less reliable; the CRNN attempts to predict a behaviourally inconsistent epoch while it is likely the RNN more flexibly captures this ambiguity by means of multiple differing fine-resolution class predictions throughout the 30 seconds.

No statistically significant variations in accuracy based on age, sex, PLMI, BMI, TST, or sleep efficiency were exhibited by the RNN 5-class ensemble model, providing an important advantage when applied in clinical contexts. The marginally significant ($p = 0.0449$) association between AHI and accuracy may

owe to the fact that individuals with sleep apnea experience sleep fragmentation, resulting in N1 sleep, one of the most difficult stages to separate; nonetheless, the association was modest ($R^2 = 0.0751$).

The series of ablation analyses establish that much of the RNN model’s performance was likely driven by chest-module features (i.e. ECG, temperature, and xyz accelerometry) rather than limb module (i.e. PPG and temperature), meaning that omitting the limb module may be reasonable if participant burden is a concern and collection of oximetry data is not necessary. Remarkably, exclusion of both ECG and PPG data with retention of only accelerometry and temperature data resulted in model performance almost indistinguishable from use of all the chest module sensors, suggesting that the inclusion of traditional heart rate sensors (PPG, ECG) is not necessary. This highlights the richness of accelerometry data obtained at the chest, spectrograms of which may capture both cardiac (ballistocardiogram) and respiratory data, as well as measures of movement. It may also contribute to the robustness of our model given the relative reliability of the accelerometers compared to the ECG/PPG sensors.

4.4 Limitations, Strengths, and Future Directions

This study had many strengths: 1) The ANNE One system itself, with multiple channels of data recorded from a pair or minimally intrusive sensors, is a strength insofar as it provides an element of redundancy should one sensor return low quality signal, 2) the inclusion of Mamba allowed the achievement of relatively high performance with a relatively parameter-scarce architecture, and 3) the study population was varied, including participants from across a spectrum of sleep disorders.

A few methodological limitations are also worth considering. 1) The differing nature of the CRNN and RNN in preprocessing and predicting (notably, the CRNN’s 30-second window as opposed to the RNN’s 1-second window) make the models difficult to compare; our reconciling of the RNN to make predictions for 30-second windows may not reflect its full performance. 2) The black box nature of CRNNs and RNNs make it difficult to ascertain the specific mechanisms used to infer sleep stage from the sensor data. Further analyses targeted toward interpreting the neural networks may be explored. 3) The recordings were overnight with a brief period of wakefulness before lights out, resulting in a preponderance of sleep vs. wake. It is difficult to know for sure how the model will perform in detecting daytime naps during long ambulatory recordings and further studies with ambulatory recordings in clinical populations will be informative. 4) The recordings were all obtained from a single site. Additional work is needed to assess the extent to which these results will be generalizable to ANNE recordings made in different settings on different patient populations.

5 Conclusion

This work introduces CRNN and RNN models to automatically perform 3-class, 4-class, and 5-class sleep staging using data from the ANNE One dual sensor using sleep stages inferred from concurrent PSG recordings, with the RNN ensemble model topping the others in virtually every performance metric. The model meets or surpasses metrics in related literature, especially for wearable devices, and demonstrates robustness across a wide range of clinical characteristics. Moreover, the model’s capability was achieved without prescreening and excluding large numbers of patients or epochs for reasons of signal quality. Compared to PSGs, the ANNE One sensor is far less intrusive of a device and procedure, which is significant for expanding the accessibility of sleep measurement for older and remote-living adults at greater risk of sleep-related illness. Our model provides a scalable, accurate minimally-intrusive approach to the ambulatory assessment of sleep staging without the need for EEG.

Acknowledgments

This research is supported by the Centre for Aging and Brain Health Innovation, Canadian Institutes of Health Research, and National Institute on Aging.

This research is not funded by Sibel Health, the manufacturer of the ANNE One device.

Special thanks to Prof. Jimmy Ba from the Department of Computer Science; Prof. Paul Kushner and Prof. Dylan Jones from the Department of Physics at the University of Toronto for offering various forms of support for this research during its infancy.

References

- [1] Alex Iranzo and Joan Santamaria. Sleep in neurodegenerative diseases. *Sleep Medicine: A Comprehensive Guide to Its Development, Clinical Milestones, and Advances in Treatment*, pages 271–283, 2015.
- [2] R.B. Berry et al. *The AASM Manual for the Scoring of Sleep and Associated Events: Rules, Terminology and Technical Specifications, Version 2.2*. American Academy of Sleep Medicine, 2015.
- [3] A Rechtschaffen and A Kales. Brain information service/brain research institute, 1968.
- [4] Syed Anas Imtiaz. A systematic review of sensing technologies for wearable sleep staging. *Sensors*, 21(5):1562, 2021.
- [5] Orestis Tsinalis, Paul M Matthews, Yike Guo, and Stefanos Zafeiriou. Automatic sleep stage scoring with single-channel eeg using convolutional neural networks. *arXiv preprint arXiv:1610.01683*, 2016.
- [6] Alexander Malafeev, Dmitry Laptev, Stefan Bauer, Ximena Omlin, Aleksandra Wierzbicka, Adam Wichniak, Wojciech Jernajczyk, Robert Riener, Joachim Buhmann, and Peter Achermann. Automatic human sleep stage scoring using deep neural networks. *Frontiers in neuroscience*, 12:781, 2018.
- [7] Hogeon Seo, Seunghyeok Back, Seongju Lee, Deokhwan Park, Tae Kim, and Kyoobin Lee. Intra-and inter-epoch temporal context network (iitnet) using sub-epoch features for automatic sleep scoring on raw single-channel eeg. *Biomedical signal processing and control*, 61:102037, 2020.
- [8] Huy Phan, Kaare Mikkelsen, Oliver Y Chén, Philipp Koch, Alfred Mertins, and Maarten De Vos. Sleeptransformer: Automatic sleep staging with interpretability and uncertainty quantification. *IEEE Transactions on Biomedical Engineering*, 69(8):2456–2467, 2022.
- [9] Ziyu Jia, Youfang Lin, Jing Wang, Ronghao Zhou, Xiaojun Ning, Yuanlai He, and Yaoshuai Zhao. Graphsleepnet: Adaptive spatial-temporal graph convolutional networks for sleep stage classification. In *Ijcai*, volume 2021, pages 1324–1330, 2020.
- [10] Luigi Fiorillo, Alessandro Puiatti, Michela Papandrea, Pietro-Luca Ratti, Paolo Favaro, Corinne Roth, Panagiotis Bargiotas, Claudio L Bassetti, and Francesca D Faraci. Automated sleep scoring: A review of the latest approaches. *Sleep medicine reviews*, 48:101204, 2019.
- [11] Huy Phan and Kaare Mikkelsen. Automatic sleep staging of eeg signals: recent development, challenges, and future directions. *Physiological Measurement*, 43(4):04TR01, 2022.
- [12] S Hochreiter. Long short-term memory. *Neural Computation MIT-Press*, 1997.
- [13] Kyunghyun Cho. Learning phrase representations using rnn encoder-decoder for statistical machine translation. *arXiv preprint arXiv:1406.1078*, 2014.
- [14] Albert Gu and Tri Dao. Mamba: Linear-time sequence modeling with selective state spaces. *arXiv preprint arXiv:2312.00752*, 2023.
- [15] Albert Gu, Isys Johnson, Karan Goel, Khaled Saab, Tri Dao, Atri Rudra, and Christopher Ré. Combining recurrent, convolutional, and continuous-time models with linear state space layers. *Advances in neural information processing systems*, 34:572–585, 2021.
- [16] Chao Zhang, Weirong Cui, and Jingjing Guo. Mssc-bimamba: Multimodal sleep stage classification and early diagnosis of sleep disorders with bidirectional mamba. *arXiv preprint arXiv:2405.20142*, 2024.
- [17] Xinliang Zhou, Yuzhe Han, Chenyu Liu, Yi Ding, Ziyu Jia, and Yang Liu. Bit-mamsleep: Bidirectional temporal mamba for eeg sleep staging. *arXiv preprint arXiv:2411.01589*, 2024.
- [18] Sibel Health. Clinical Care | ANNE One. URL <https://sibelhealth.com/clinical-care/>.
- [19] Pin-Wei Chen, Megan K O’Brien, Adam P Horin, Lori L McGee Koch, Jong Yoon Lee, Shuai Xu, Phyllis C Zee, Vineet M Arora, and Arun Jayaraman. Sleep monitoring during acute stroke rehabilitation: Toward automated measurement using multimodal wireless sensors. *Sensors*, 22(16): 6190, 2022.
- [20] Mustafa Radha, Pedro Fonseca, Arnaud Moreau, Marco Ross, Andreas Cerny, Peter Anderer, Xi Long, and Ronald M Aarts. Sleep stage classification from heart-rate variability using long short-term memory neural networks. *Scientific reports*, 9(1):14149, 2019.

- [21] Haoqi Sun, Wolfgang Ganglberger, Ezhil Panneerselvam, Michael J Leone, Syed A Quadri, Balaji Goparaju, Ryan A Tesh, Oluwaseun Akeju, Robert J Thomas, and M Brandon Westover. Sleep staging from electrocardiography and respiration with deep learning. *Sleep*, 43(7):zsz306, 2020.
- [22] Kevin Kotzen, Peter H Charlton, Sharon Salabi, Lea Amar, Amir Landesberg, and Joachim A Behar. Sleepppg-net: A deep learning algorithm for robust sleep staging from continuous photoplethysmography. *IEEE Journal of Biomedical and Health Informatics*, 27(2):924–932, 2022.
- [23] Nicolò Pini, Ju Lynn Ong, Gizem Yilmaz, Nicholas IYN Chee, Zhao Siting, Animesh Awasthi, Siddharth Biju, Kishan Kishan, Amiya Patanaik, William P Fifer, et al. An automated heart rate-based algorithm for sleep stage classification: Validation using conventional polysomnography and an innovative wearable electrocardiogram device. *Frontiers in Neuroscience*, 16:974192, 2022.
- [24] Pavlos I Topalidis, Sebastian Baron, Dominik PJ Heib, Esther-Sevil Eigl, Alexandra Hinterberger, and Manuel Schabus. From pulses to sleep stages: Towards optimized sleep classification using heart-rate variability. *Sensors*, 23(22):9077, 2023.
- [25] Adam M Jones, Laurent Itti, and Bhavin R Sheth. Expert-level sleep staging using an electrocardiography-only feed-forward neural network. *Computers in Biology and Medicine*, 176:108545, 2024.
- [26] Kianoosh Kazemi, Arash Abiri, Yongxiao Zhou, Amir Rahmani, Rami N Khayat, Pasi Liljeberg, and Michelle Khine. Improved sleep stage predictions by deep learning of photoplethysmogram and respiration patterns. *Computers in Biology and Medicine*, 179:108679, 2024.
- [27] Fernanda B Silva, Luisa FS Uribe, Felipe X Cepeda, Vitor FS Alquati, João PS Guimarães, Yuri GA Silva, Orlem L Dos Santos, Alberto A de Oliveira, Gabriel HM de Aguiar, Monica L Andersen, et al. Sleep staging algorithm based on smartwatch sensors for healthy and sleep apnea populations. *Sleep Medicine*, 119:535–548, 2024.
- [28] Xin Zhang, Weixuan Kou, I Eric, Chao Chang, He Gao, Yubo Fan, and Yan Xu. Sleep stage classification based on multi-level feature learning and recurrent neural networks via wearable device. *Computers in biology and medicine*, 103:71–81, 2018.
- [29] Leland McInnes, John Healy, Steve Astels, et al. hdbscan: Hierarchical density based clustering. *J. Open Source Softw.*, 2(11):205, 2017.
- [30] Andrew Zhang, Chunlin Li, Yuzhi Tang, Alex He-Mo, Nasim Montazeri Ghahjaverestan, Maged Goubbran, and Andrew Lim. 1122 a deep learning model for inferring sleep stage from a flexible wireless dual sensor wearable system without eeg. *Sleep*, 47(Supplement_1):A481–A482, 2024.
- [31] Vincent Theodoor Van Hees, Severine Sabia, Samuel E Jones, Andrew R Wood, Kirstie N Anderson, M Kivimäki, Timothy M Frayling, Allan I Pack, Maja Bucan, MI Trenell, et al. Estimating sleep parameters using an accelerometer without sleep diary. *Scientific reports*, 8(1):12975, 2018.
- [32] Diederik P. Kingma and Jimmy Lei Ba. Adam: A method for stochastic optimization. In *3rd International Conference for Learning Representations*, January 2017.
- [33] Yoav Freund and Robert E Schapire. A decision-theoretic generalization of on-line learning and an application to boosting. In *European conference on computational learning theory*, pages 23–37. Springer, 1995.
- [34] Tin Kam Ho. The random subspace method for constructing decision forests. *IEEE transactions on pattern analysis and machine intelligence*, 20(8):832–844, 1998.
- [35] Pierre Geurts, Damien Ernst, and Louis Wehenkel. Extremely randomized trees. *Machine learning*, 63:3–42, 2006.
- [36] Jingyi Cui, Hanyuan Hang, Yisen Wang, and Zhouchen Lin. Gbht: Gradient boosting histogram transform for density estimation. In *International Conference on Machine Learning*, pages 2233–2243. PMLR, 2021.
- [37] Tianqi Chen and Carlos Guestrin. Xgboost: A scalable tree boosting system. In *Proceedings of the 22nd acm sigkdd international conference on knowledge discovery and data mining*, pages 785–794, 2016.
- [38] Leland McInnes, John Healy, and James Melville. Umap: Uniform manifold approximation and projection for dimension reduction. *J. Open Source Softw.*, 3(29):861, 2018.

Appendix A: Summary Statistics by Groups

Table 7. Sleep variables of study participants stratified by age and sleep apnea with t-test p -values to indicate the differences' significances. Values are formatted as mean \pm standard deviation.

<i>Variable</i>	<i>Age ≥ 65</i>	<i>Age < 65</i>	<i>p</i>	<i>AHI ≥ 5</i>	<i>AHI < 5</i>	<i>p</i>
Age [y]				64.01 \pm 14.34	51.82 \pm 18.07	1.48 $\times 10^{-11}$
Sex [% Female]	44.52 \pm 49.70	52.83 \pm 49.92	0.123	40.36 \pm 49.06	57.29 \pm 49.47	1.34 $\times 10^{-3}$
AHI	14.23 \pm 16.64	9.90 \pm 17.59	0.0203			
TST [h]	4.61 \pm 1.29	5.43 \pm 1.48	1.46 $\times 10^{-7}$	4.86 \pm 1.35	5.30 \pm 1.52	4.82 $\times 10^{-3}$
PLMI	23.34 \pm 35.41	9.22 \pm 16.82	7.96 $\times 10^{-7}$	16.64 \pm 25.38	13.55 \pm 28.18	0.281
Body Mass Index	27.89 \pm 4.59	27.90 \pm 6.19	0.986	29.45 \pm 5.72	26.55 \pm 5.13	7.54 $\times 10^{-7}$
Sleep Efficiency [%]	65.81 \pm 16.40	75.84 \pm 17.81	1.27 $\times 10^{-7}$	69.61 \pm 17.48	73.61 \pm 18.13	0.0356
Awake [%]	46.64 \pm 15.00	37.10 \pm 16.47	5.22 $\times 10^{-8}$	43.01 \pm 16.08	39.25 \pm 16.78	0.0321
N1 Sleep [%]	12.13 \pm 6.64	10.43 \pm 5.83	0.0110	13.15 \pm 6.97	9.37 \pm 4.88	5.41 $\times 10^{-9}$
N2 Sleep [%]	25.87 \pm 10.31	30.06 \pm 10.46	2.17 $\times 10^{-4}$	26.77 \pm 11.03	29.72 \pm 10.02	8.59 $\times 10^{-3}$
N3 Sleep [%]	8.20 \pm 6.73	12.64 \pm 8.48	2.38 $\times 10^{-7}$	9.00 \pm 7.43	12.41 \pm 8.34	6.36 $\times 10^{-5}$
REM Sleep [%]	7.16 \pm 5.20	9.77 \pm 6.40	5.96 $\times 10^{-5}$	8.07 \pm 5.84	9.25 \pm 6.22	0.0679

Appendix B: Bidirectional Mamba Block

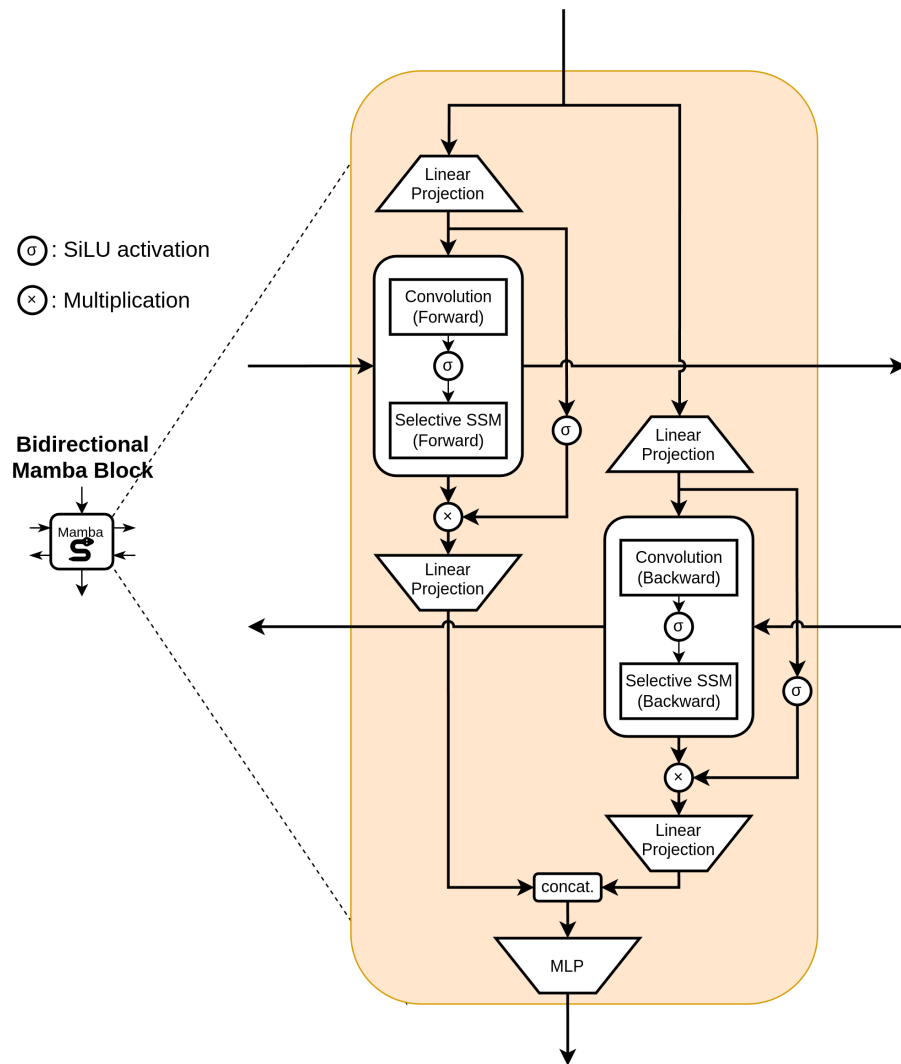


Figure 8. Detailed architecture of the bidirectional Mamba block illustrated in Figure 2.

Appendix C: Explorations in Feature Selection

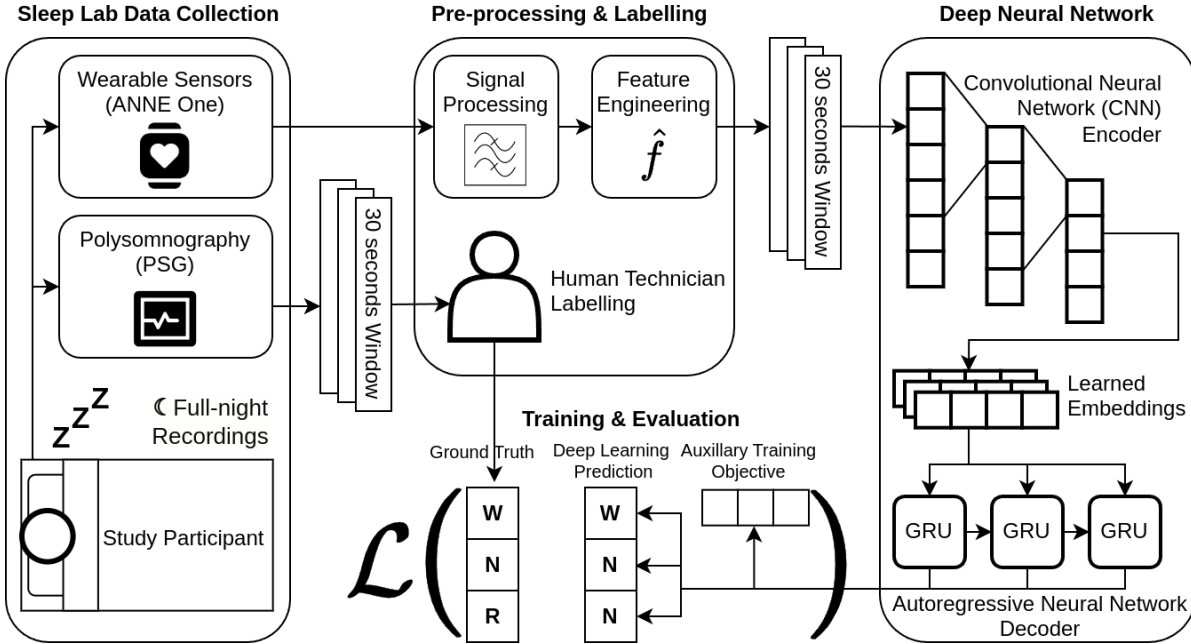


Figure 9. The overall deep learning pipeline and architecture of the earlier study, as presented at *SLEEP 2024* [30] at Houston, Texas in May 2024.

A previous iteration of the model used a pure CRNN (GRU) approach, and the approach encompassed two additional strategies, which are utilized within the paper without extensive justification.

The *engineered features* are a suite of additional features across the time, frequency, and scalar domains used alongside the raw signals as extracted from the ANNE sensors.

Table 8. Engineered features in the *Appendix C* approach

Time Domain	Frequency Domain	Scalar Domain
PPG, ECG Heart Rates	PPG Freq. Spectra	PPG Freq. Spectra Skew
PPG, ECG Signal Quality Index	ECG Freq. Spectra	PPG Time Entropy
PPG, ECG Amplitude	x-accel. Freq. Spectra	PPG Freq. Spectra Entropy
Pulse Arrival Time (PAT)	y-accel. Freq. Spectra	$ \Delta \text{Heart Rate} $
Accel. ENMO	z-accel. Freq. Spectra	Accel. ENMO Kurtosis
SpO2		Accel. z-angle Freq. Spectra Entropy
		Metadata (Gender, Age)

In addition, the *auxiliary training objective* was introduced in the form of the transition state. These states are derived directly from the target labels. With this, the model attempts to predict whether there will be a change in sleep class from this epoch to the next. The rationale is that sleep stages in reality do not always change at the end of 30-second windows, and many epochs may have data that is transitioning between two separate sleep stages, which would be difficult for the model as they may not resemble other members of their labelled class and instead as a mixture of both sleep stages. By training the model to also predict correct transitions, it should assist the model in determining which epochs may be occurring during a transition between stages, and thus make it more robust in general.

The application of the transition state as an auxiliary objective was attempted in the Mamba approaches in the main paper; however, it did not yield a noticeable increase in performance, and thus was not included in the final models.

The results of the approach are detailed in the graph below, with results indicating that the two approaches mentioned positively impacted results.

Table 9. Evaluation performance of *Appendix C* deep learning models for 3-class sleep staging and 2-class sleep detection

	3-Class Sleep Staging			2-Class Sleep Detection		
	F1	Precision	Accuracy	F1	Precision	Accuracy
Wake						
Time Series Only Baseline	0.681	0.723	0.644	0.740	0.649	0.860
Engineered Features	0.743	0.723	0.764	0.742	0.703	0.786
Engineered Features & Auxiliary Objective	0.727	0.757	0.700	0.781	0.701	0.880
Ensemble	0.732	0.789	0.683			
NREM			Sleep			
Time Series Only Baseline	0.534	0.720	0.425	0.793	0.892	0.714
Engineered Features	0.507	0.754	0.381	0.826	0.859	0.826
Engineered Features & Auxiliary Objective	0.619	0.744	0.530	0.834	0.912	0.769
Ensemble	0.702	0.767	0.647			
REM						
Time Series Only Baseline	0.401	0.265	0.827			
Engineered Features	0.428	0.287	0.844			
Engineered Features & Auxiliary Objective	0.447	0.314	0.778			
Ensemble	0.517	0.381	0.679			
Macro						
Time Series Only Baseline	0.539	0.632	0.555	0.767	0.771	0.770
Engineered Features	0.559	0.663	0.581	0.783	0.784	0.792
Engineered Features & Auxiliary Objective	0.600	0.598	0.624	0.807	0.807	0.811
Ensemble	0.651	0.646	0.679			

Appendix D: Scalar and Frequency Features

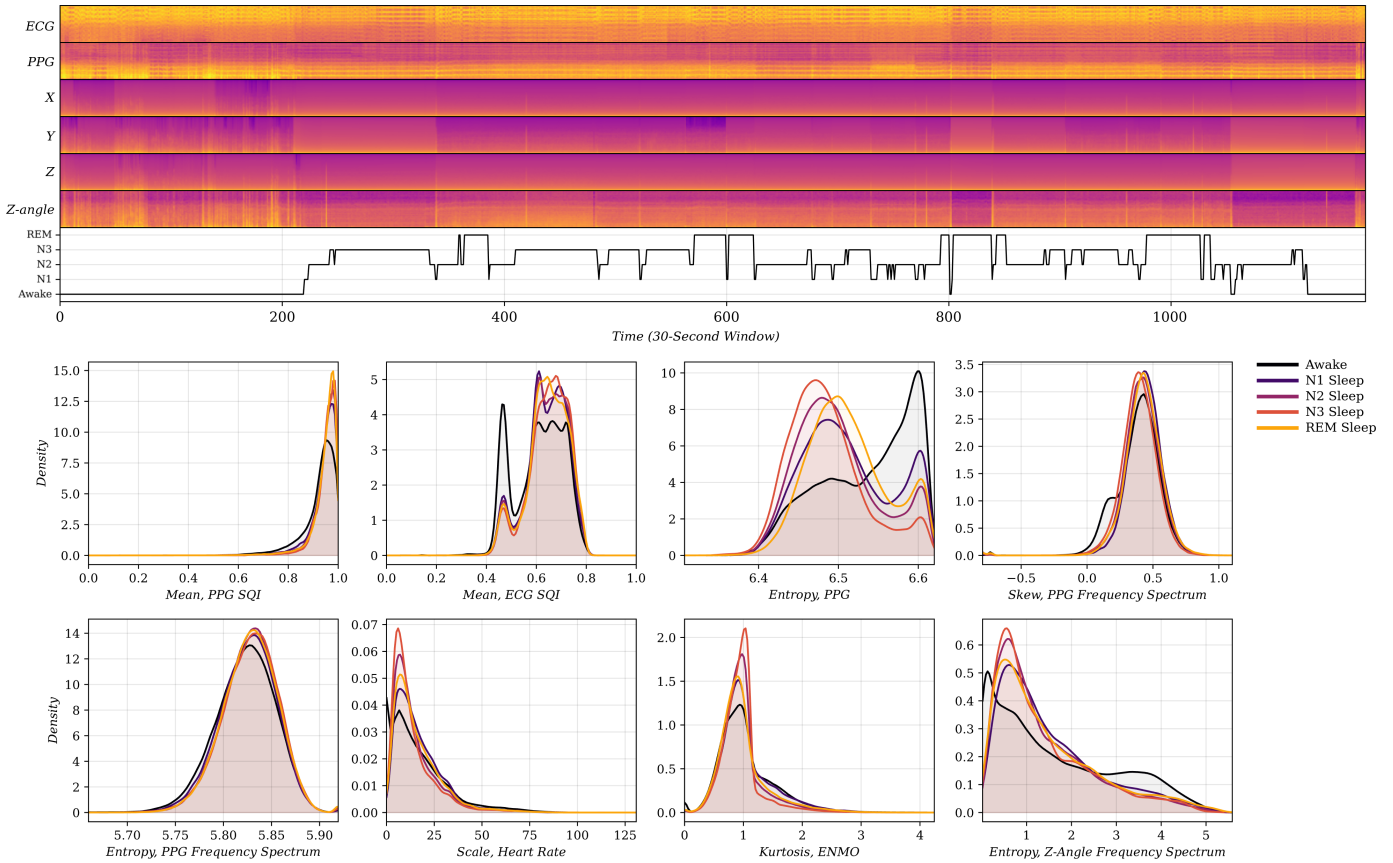


Figure 10. Top. Kernel density estimations of the distributions of engineered scalar features by sleep stage across the dataset used for this study; **Bottom.** Spectrograms of frequency domain features aligned to the ground truth sleep stages of a participant in our study.

Appendix E: UMAP of CRNN Model Learned Embeddings

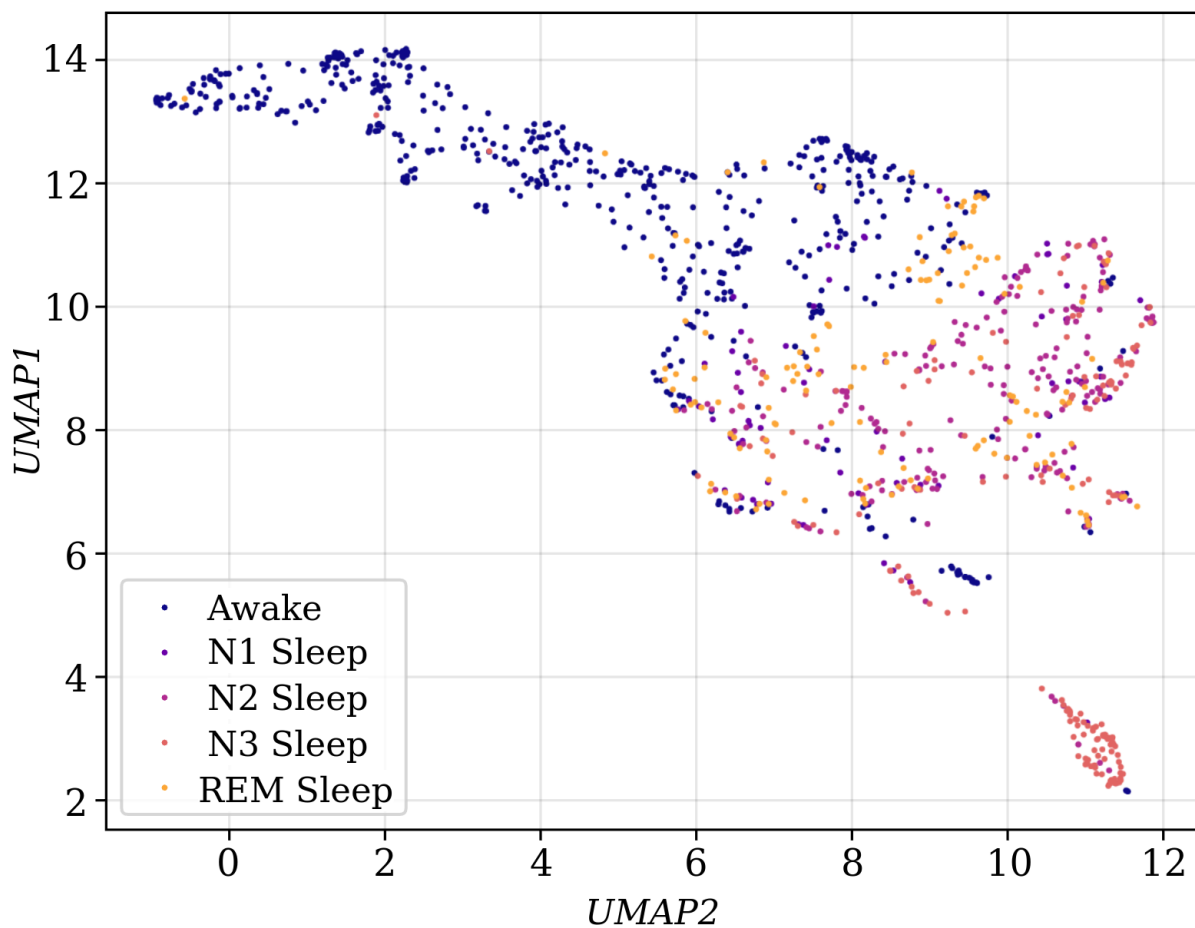


Figure 11. UMAP projection of concatenated times-series and frequencies embedding vectors of the 5-class CRNN model for a single full-night recording for a participant in the test set, colored by ground truth sleep stage. This is for the same recording as displayed on Figure 4.

Appendix F: Class-Wise Evaluation Metrics

Table 10. Class-wise metrics for all n -class models on the test set, calculated by the metrics as applied to binary labels indicating the presence or absence of a given class. The best-performing model for each metric is bolded.

<i>Metric (%)</i>	<i>5-Class Sleep Staging</i>				<i>4-Class Sleep Staging</i>				<i>3-Class Sleep Staging</i>			
	Regular		Ensemble		Regular		Ensemble		Regular		Ensemble	
	CRNN	RNN	CRNN	RNN	CRNN	RNN	CRNN	RNN	CRNN	RNN	CRNN	RNN
	Wake				Wake				Wake			
Balanced Accuracy	83.75	84.93	86.47	86.19	84.13	86.12	87.93	87.87	78.57	88.14	87.97	88.27
Precision	84.61	88.16	87.64	88.44	84.48	88.57	88.34	88.67	80.48	88.70	88.24	88.82
Recall	84.68	87.28	87.64	88.04	83.38	88.07	88.32	88.70	76.26	88.72	88.12	88.85
F1	84.63	86.93	87.54	87.81	83.53	87.82	88.33	88.66	76.40	88.71	88.16	88.83
Cohen's κ	67.92	72.53	73.93	74.41	66.37	74.42	75.74	76.32	53.63	76.47	75.45	72.89
MCC	67.95	73.94	74.11	75.17	67.04	75.32	75.74	76.37	56.43	76.48	75.49	76.74
	N1 Sleep				N1/N2 Sleep				Non-REM Sleep			
Balanced Accuracy	62.71	65.07	67.99	69.62	69.22	67.11	71.58	73.47	72.35	83.46	81.03	85.42
Precision	85.30	85.70	86.74	87.09	73.32	68.97	75.37	75.61	74.26	83.60	81.90	85.50
Recall	82.64	78.13	81.74	79.31	73.05	69.43	75.06	75.81	72.28	83.45	80.99	85.41
F1	83.84	81.14	83.77	82.25	71.73	69.01	74.00	75.36	71.73	83.43	80.87	85.41
Cohen's κ	21.74	20.73	27.21	26.46	40.67	34.97	45.39	48.25	44.64	66.90	62.01	70.83
MCC	22.12	22.58	28.61	29.06	42.52	35.19	47.03	48.74	46.54	67.05	62.90	70.92
	N2 Sleep											
Balanced Accuracy	64.85	67.47	65.88	67.72								
Precision	73.86	74.95	76.25	76.33								
Recall	75.49	76.27	77.22	77.50								
F1	73.44	75.03	74.80	75.82								
Cohen's κ	33.51	37.98	36.71	39.58								
MCC	35.28	38.87	39.68	41.29								
	N3 Sleep				N3 Sleep							
Balanced Accuracy	76.48	78.15	79.40	81.16	77.36	81.50	80.08	82.18				
Precision	89.80	90.53	90.86	91.71	90.46	90.98	90.92	91.72				
Recall	85.36	87.47	87.60	89.66	88.07	81.92	86.85	88.59				
F1	87.03	88.64	88.82	90.45	89.02	84.87	88.32	89.72				
Cohen's κ	39.73	45.03	46.36	52.35	45.54	38.84	45.47	50.70				
MCC	41.84	46.52	48.08	53.44	46.58	44.30	47.77	52.60				
	REM Sleep				REM Sleep				REM Sleep			
Balanced Accuracy	75.29	81.55	82.31	86.60	77.83	77.66	82.99	88.67	70.09	85.57	84.13	89.26
Precision	90.95	93.38	92.70	94.69	91.67	93.31	92.63	94.97	90.33	93.47	92.52	94.87
Recall	90.33	93.24	91.39	94.31	90.93	93.76	90.70	94.26	91.04	91.80	89.04	93.81
F1	90.61	93.31	91.91	94.46	91.26	93.46	91.42	94.52	90.63	92.40	90.25	94.18
Cohen's κ	47.59	61.83	56.59	69.06	51.59	60.63	55.18	70.06	43.76	60.09	51.95	68.78
MCC	47.72	61.85	57.27	69.23	51.80	61.06	56.35	70.54	44.03	61.23	54.38	69.61

Appendix G: Additional Model Performance Plots

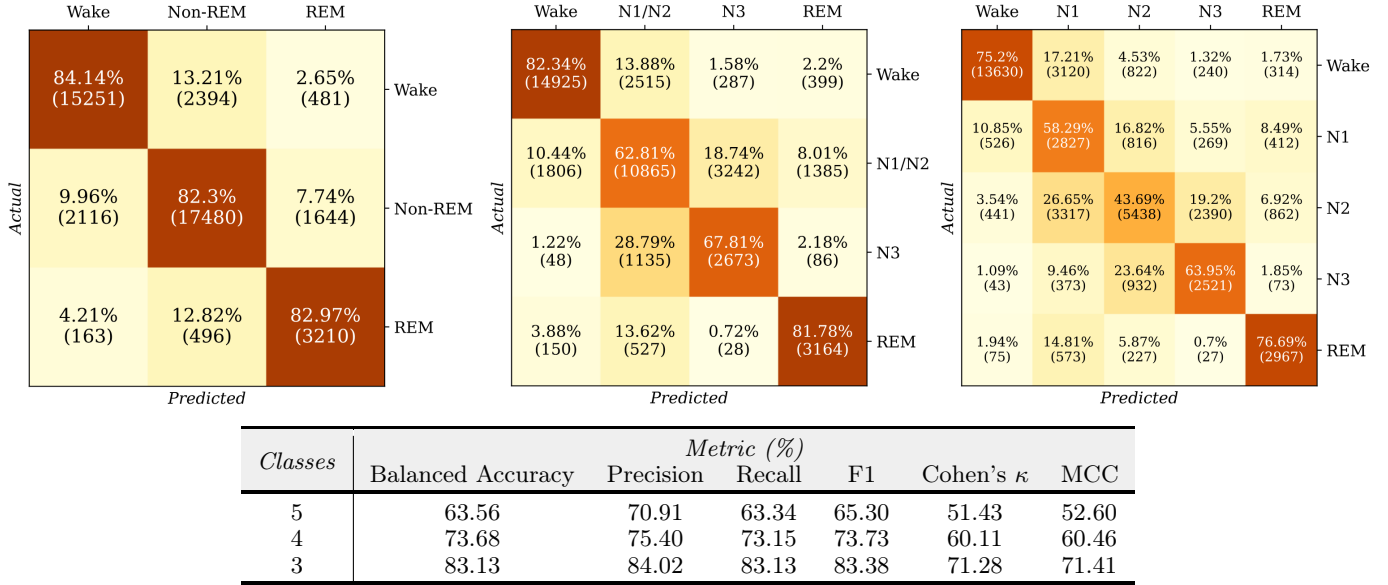


Figure 12. Confusion matrices and macro-evaluation metrics of 3-class, 4-class, and 5-class RNN ensemble models after filtering out the healthy subset of the test set ($n = 43$), defined as age ≥ 40 or AHI ≥ 5 or PLMI ≥ 5 .

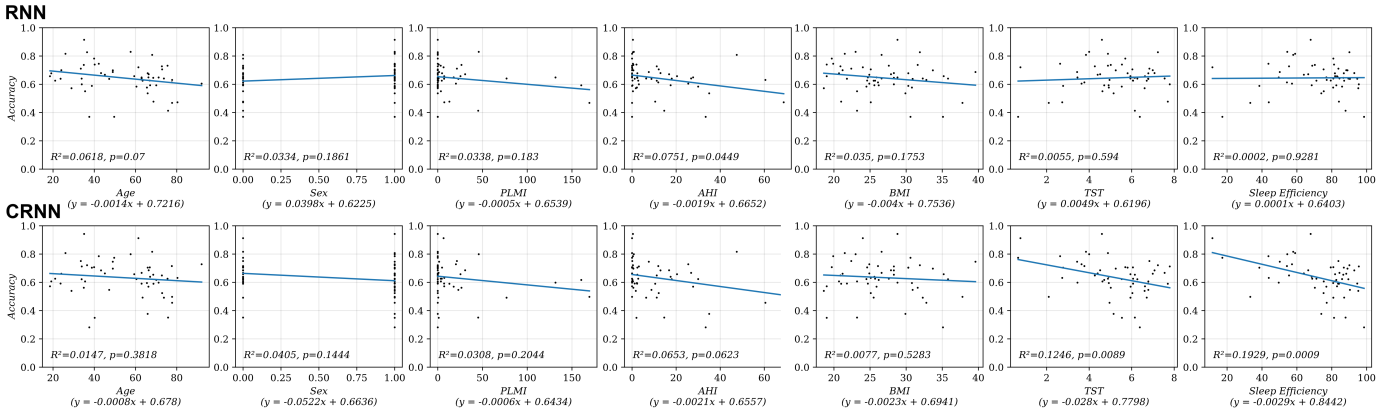


Figure 13. Scatter plots of recording-wise accuracy against clinical metrics comprising age, sex, PLMI, AHI, BMI, TST, and sleep efficiency for recordings in the test set. A linear regression line is plotted, with its equation, R^2 , and p -value of slope provided below.